nature communications

Article

https://doi.org/10.1038/s41467-025-62539-7

On-chip integration of achromatic metalens arrays

Received: 12 December 2024

Accepted: 23 July 2025

Published online: 12 August 2025

Check for updates

Yao Zhang[1], Xiong Jiang[1], Geyang Qu[1], Jing Han[1], Chen Li[1], Baichuan Bo[1], Qifeng Ruan[1], Zhengtong Liu[2], Qinghai Song[1,2,3] & Shumin Xiao[1,2,3]

Broadband achromatic metalenses and metalens arrays hold promise for enabling high-performance optical imaging in a compact form factor. Conventional visible-light achromatic metalenses are composed of transparent and high-refractive-index TiO_2 or GaN nanopillars, but are strongly limited in mainstream silicon-based complementary metal-oxide-semiconductor (CMOS) processes. Herein, we report the realization of high-efficiency Si_3N_4 achromatic metalenses in the visible range and demonstrate their integration onto a commercial imaging chip. By improving nanofabrication techniques, we have dramatically increased the aspect ratio of Si_3N_4 nanostructures from ~17 to a high value of 43.33. Consequently, the group delay of the Si_3N_4 nanostructures is significantly increased and the averaged focusing efficiency of a Si_3N_4 metalens with a numerical aperture of 0.155 reaches 80.39%. Owing to the CMOS-compatibility of Si_3N_4, such high-quality metalenses have been integrated with commercial imaging sensors and demonstrated the capability of full-color optical imaging. This research paves a critical step towards chip-integrated meta-devices.

Lenses are integral components of optical systems and are widely used in many industries including automotive, electronics, healthcare and telecommunications. The rapid development of emerging technologies such as medical imaging and augmented reality has brought about the demand for ultracompact and integrated optical lenses, and has spawned the research field of metalenses[1–9]. Metalens is a planar photonic device that is composed of nanoantennas and has the diffraction-limited focusing capabilities[10–19]. In principle, the periodic lattice and optical resonances greatly increase the dispersion of the metalens, leading to more severe chromatic aberration than its bulky counterpart[20–22]. Soon after the advent of metalenses, chromatic aberration has attracted considerable research attention and great efforts were made to eliminate it. In 2018, using high-refractive-index dielectrics such as TiO_2 and GaN, the visible-light broadband achromatic metalens was experimentally demonstrated, and a series of applications such as full-color imaging, light-field imaging, and hyperspectral imaging were developed from this[23–28]. Despite the progress in miniaturization of optical system, the deposition of TiO_2 and GaN membranes typically requires temperature higher than 600 °C, strongly restricting the direct integration of such metalens on top of conventional integrated circuits (IC) chip[29,30].

Silicon nitrides (Si_3N_4) is another transparent material with a high refractive index in the visible light range. High quality Si_3N_4 membrane can be deposited with plasma enhanced chemical vapor deposition (PECVD) at a relatively low temperature[31,32]. Meanwhile, Si_3N_4 nanostructures can be easily achieved with conventional processes of the mature IC industry[33–35]. As a consequence, Si_3N_4 has been widely used in various microelectronic and photonic chips. It is also a reasonable idea to use Si_3N_4 to prepare achromatic metalenses. On the one hand, Si_3N_4 is compatible with CMOS and can be mass-produced, which can greatly reduce the cost of achromatic metalenses and bring their prices close to the price range of traditional optical devices. On the other hand, low-temperature processing technology allows achromatic metalenses to be directly integrated into traditional IC chips, which will

[1]Ministry of Industry and Information Technology Key Lab of Micro-Nano Optoelectronic Information System, Harbin Institute of Technology Shenzhen, Shenzhen 518055, PR China. [2]Pengcheng Laboratory, Shenzhen, Guangdong 518055, PR China. [3]Collaborative Innovation Center of Extreme Optics, Shanxi University, Taiyuan, Shanxi 030006, PR China. e-mail: qinghai.song@hit.edu.cn; shumin.xiao@hit.edu.cn

greatly promote the practical application of such planar photonic devices. Although some efforts have been made recently, the device performances of Si_3N_4 achromatic metalenses are still restricted. This is because the refractive index of Si_3N_4 is much lower than TiO_2 and GaN, and the nanofabrication technique only allows an aspect ratio around 10-17[36–41]. The library of meta-atom is thus strongly limited and the transmittance (focusing efficiency) must be sacrificed to fulfill the required group delay[42,43]. So far, high-performance Si_3N_4 achromatic metalenses remain technically challenging and absent (details in Supplementary Note 1). Here, we report the improvement of Si_3N_4 nanofabrication technique and the realization of high-efficiency Si_3N_4 achromatic metalenses in the visible range. Their direct integration onto a commercial imaging chip and the corresponding full-color imaging have also been demonstrated.

Results

Numerical design of Si_3N_4 achromatic metalens

Figure 1(a) illustrates a schematic diagram of the integrated imaging system. It is an achromatic metalens integrated onto a commercial CMOS imaging sensor. The metalens is composed of Si_3N_4 nanopillars with different profiles that can support a spatial and frequency-dependent phase profiles following the equation[24]

$$\varphi(r,\omega) = -\frac{\omega}{c}\left(\sqrt{r^2+F^2}-F\right), \tag{1}$$

where c, r, ω, and F are the speed of light, radial coordinates, angular frequency, and focal length, respectively. To achieve achromatic focusing within a frequency range around ω_d, it is well-known that both the relative phase $\varphi(r,\omega_d)$ and relative group delay $\partial\varphi(r,\omega)/\partial\omega$ should be satisfied at least. In principle, when the extremes of dispersion are represented at the center and edge of the metalens, the required range of group delay is defined as the group delay difference at the center and edge of the metalens, which is closely related to the numerical aperture (NA), the radius, and achromatic bandwidth of the metalens. Consequently, the minimal group delay is determined once the NA and size of achromatic metalens are pre-defined (details in Supplementary Note 2).

In design, both the phase and group delay are provided by Si_3N_4 nanopillars. Without considering the mode coupling and end-facet reflection, the phase of transmitted light through each Si_3N_4 nanopillar can be simplified to $\varphi(r,\omega)=\frac{\omega}{c}n_{eff}h$, where n_{eff} and h are the effective refractive index and the pillar height. Then the group delay at position r can be expressed as

$$\frac{\partial\varphi(r,\omega)}{\partial\omega} = \frac{1}{c}n_{eff}h + \frac{\omega}{c}\frac{\partial n_{eff}}{\partial\omega}h. \tag{2}$$

It is obvious that both the phase and the range of relative group delay is proportional to the product of the effective refractive index and pillar height. The effective refractive index is determined by the ratio of electromagnetic waves inside dielectrics and in air and varies between n = 1 (air) and n ~ 2 (Si_3N_4) by controlling the in-plane morphology of nanopillar. As a consequence, the group delay range and corresponding size and NA of the achromatic metalens depends directly on the pillar height and aspect ratio. The group delay dispersion (GDD, which means the derivative of group delay with respect to diagonal frequency) will also increase by increasing the height to 1300 nm. However, the linear fitting metric R^2_{linear} for all the selected nanopillars keeps exceed 0.997, confirming that the influence of GDD is smaller and can be not considered within the 200 nm bandwidth centered at 510 nm in our design.

In numerical simulation, ten types of meta-units, including squares, circles, crosses, concentric overlays of circles and crosses, petal shapes and their corresponding anti-structures were employed as building blocks of the metalens (Fig. 1b). Each shape has at least C4 rotational symmetry and thus the dependence on the incident polarization has been eliminated. Parameter sweeps of the meta-units size and shape were conducted to build a library that provides values for phase, group delay, and transmittance in the entire visible spectrum with a step of 2 nm (see three examples in Supplementary Fig. S2). For the fixed shapes, the increase of pillar height has a double advantage. It

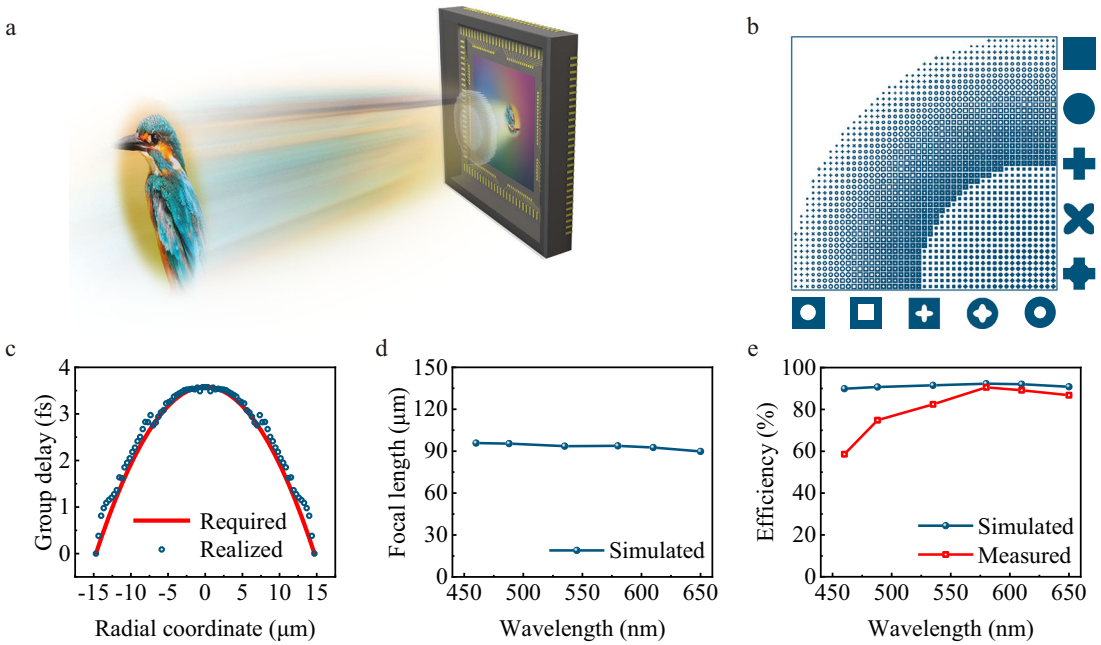

Fig. 1 | The design and the performance of the Si_3N_4 achromatic metalens. **a** Schematic of the broadband Si_3N_4 achromatic metalens showing the principle of integral imaging. **b** The layout of the quarter of the designed metalens. Ten fundamental building blocks are enlarged at the edge. **c** The required group delay for broadband achromatic metalens with NA = 0.155 (solid line) and the values provided by the Si_3N_4 meta-units (dots). **d** Numerically calculated focal length of the metalens at different wavelengths. **e** Numerically calculated (dots) and experimental measured (squares) efficiency of the metalens at different wavelengths. The diameter of metalens is fixed at 30 μm.

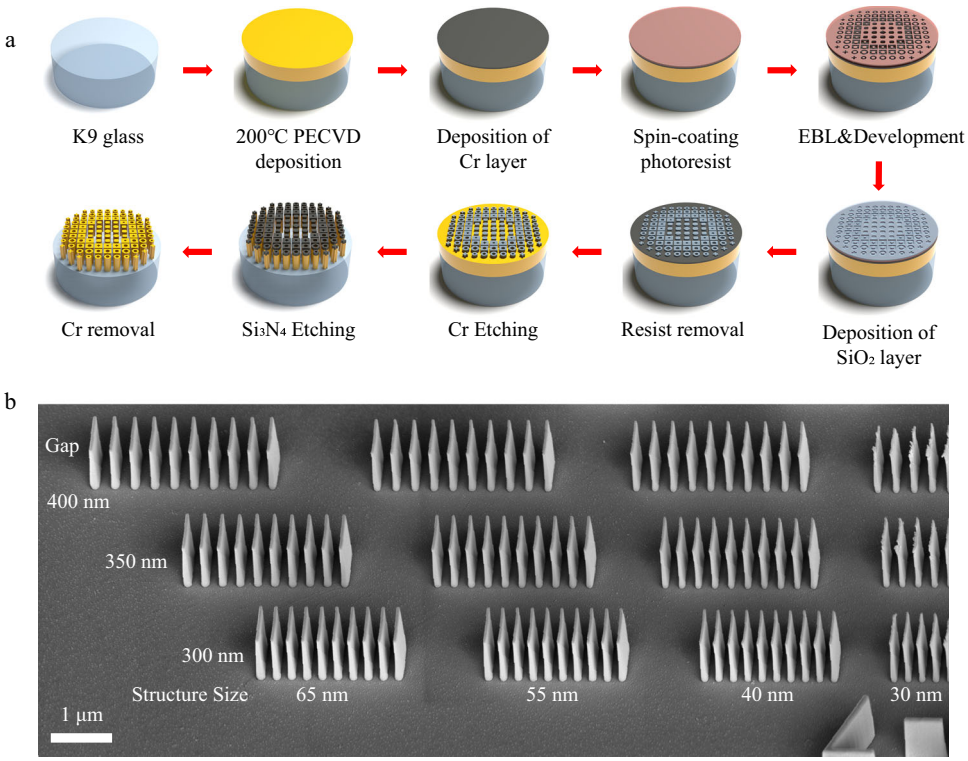

Fig. 2 | Fabrication of high-quality Si_3N_4 nanostructures. a Schematic diagram of the nanofabrication process. **b** The tilt-view SEM images of grating arrays with different duty cycles. The width of each nano-ridge reduces from 65 nm to 30 nm, respectively.

greatly enlarges the range of group delay (Supplementary Fig. S3) and allows a better fitting to the required values. Meanwhile, more nanopillars can provide similar phase and group delay and thus a higher transmittance can also be selected, closely relating to the focusing efficiency of achromatic metalens.

To fit the nanofabrication capability, we restrict the pillar height to h = 1300 nm and the minimal feature size to 40 nm. Figure 1c–e shows the numerical results of an achromatic metalens with a NA of 0.155. It is obviously that the required group delay has been satisfied (Fig. 1c). As a consequence, the incident light with wavelength from 460 nm to 650 nm have been focused to the same position around F = 93.5 μm with a variation below 1.6% (Fig. 1d). Figure 1e shows the numerically calculated focusing efficiency (the ratio of the energy at the focus to the energy at the incident beam) across the visible spectrum. We can see that the efficiency varies slightly around 90% and gives an average value of 91.2%. All these results are consistent with the above analysis and demonstrate that high-performance visible-light achromatic metalens can also be realized with Si_3N_4 if the nanofabrication technique is improved to ensure the designed pillar height and aspect ratio (comparison details with other metalenses are shown in Supplementary Note 1).

Fabrication of high quality Si_3N_4 metalens

A crucial step towards high-performance Si_3N_4 achromatic metalens lies in the nanofabrication technology. Recent progress shows Si_3N_4 nanostructures with height up to 1250 nm can be fabricated[38]. The aspect ratio, however, is only around 10 to 17, resulting in a restricted focusing efficiency (36–55%) and a small NA of 0.086[13]. To realize the designed meta-devices, we have developed a top-down etching technology. The Si_3N_4 film is deposited at a low temperature of 200 °C using plasma enhanced chemical vapor deposition (PECVD, Oxford PlasmaPro 800). The deposition temperature is strictly controlled to be below 250 °C to prevent damage to the imaging detector on the wafer when preparing metasurfaces on CMOS surface in the future. The refractive index and light extinction coefficient are shown in Supplementary Fig. S5. The refractive index of Si_3N_4 film exceeds 2.02 in 460–650 nm wavelength range, while the light extinction coefficient approaches zero. All these results show that the Si_3N_4 film deposited at a low temperature is suitable for high-performance meta-devices.

The Si_3N_4 nanostructures are fabricated with a combined process of electron-beam (E-Beam) lithography and inductively coupled plasma (Oxford Plasmalab System 100, ICP180) etching. The schematic of fabrication is shown in Fig. 2a. In the first, a 50 nm Cr layer was deposited on it by electron beam evaporation. Next, the nanostructures were patterned using E-beam lithography and transferred to SiO_2 via a typical lift-off process. The pattern was further transferred into the Cr layer using an ICP etching process with a selectivity up to 100:1. Then Si_3N_4 membrane was etched in ICP by taking Cr layer as a hard mask. Different from previous demonstrations, our approach uses the mixture of CHF_3 and O_2. The introduction of O and H ions can induce C and F ions to form a fluorocarbon protective layer on the Si_3N_4 surface, thereby achieving simultaneous etching and deposition, effectively reducing the surface roughness. Meanwhile, we dynamically adjust the ratio of CHF_3 and O_2 from 12.5 to 7.2 as depth increases so that fluorocarbons exist at a relatively stable thickness. This adjustment can effectively prevent the accumulation of fluorocarbon in the micro-grooves and maintain the anisotropy of the etching process. As a result, high quality Si_3N_4 nanostructures can be obtained (details in Supplementary Note 4).

Taking the gratings as an example, we have tested our fabrication process. Figure 2b shows the tilt-view scanning electron microscope (SEM) images of Si_3N_4 gratings. Here the pillar height is 1300 nm. High quality Si_3N_4 nanostructures can be preserved by reducing the width of nano-ridges from ~ 65 nm to 30 nm. Obvious collapse of Si_3N_4 nanostructures can be found when the width of nano-ridge is below 20 nm. Similar high-quality nanofabrication is also applicable to two dimensional materials, e.g., Si_3N_4 nanopillars with different geometries (see Supplementary Fig. S8). Therefore, we can confirm that our process

https://doi.org/10.1038/s41467-025-62539-7

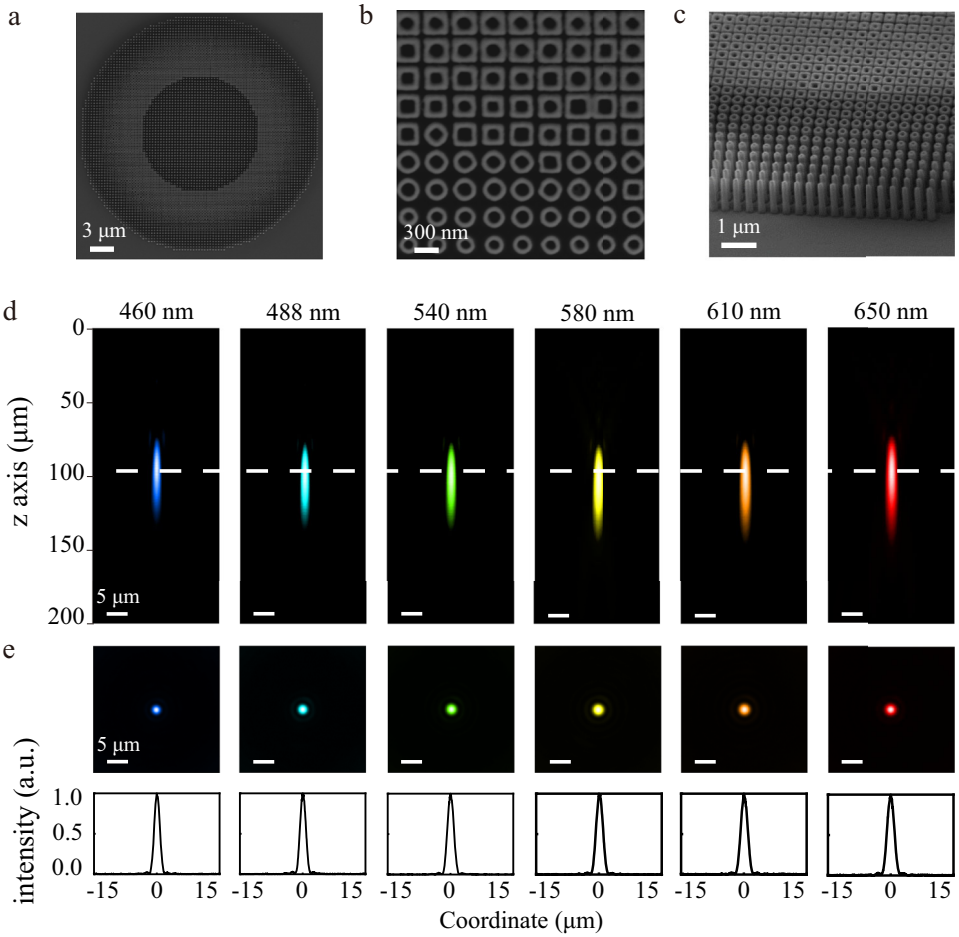

Fig. 3 | The experimentally fabricated Si_3N_4 metalens with NA = 0.155. a, **b** are the top-view SEM images of achromatic metalens with different resolutions. Different types of meta-units can be clearly identified. **c** The corresponding tilt-view SEM image of the metalens. **d**, **e** are the intensity profiles of focal spots in x-z plane and x-y planes at different wavelengths. The white dashed line depicts the numerical focal length. The bottom panels depict the normalized intensity profiles along the diameter. The intensity profiles have the same scale bar.

has the capability of fabricating Si_3N_4 nanostructures with a thickness of 1300 nm. The aspect ratio is calculated by fabricating a series of gratings with width from 65 nm to 30 nm and aspect ratio is calculated to 43.33 (see Supplementary Fig. S9-10 and Supplementary Movie 1). Compared to other top-down fabrication, this approach can provide a record high aspect ratio. Meanwhile, it offers significant advantages of meta-devices by being directly implemented on packaged CMOS detectors. This capability makes the process low-cost and semiconductor foundry compatibility, presenting considerable benefits for the development of flat optical systems in real applications.

Characterization of Si_3N_4 achromatic metalens

With the same process, the designed metalenses in Fig. 1 have been experimentally fabricated. Figure 3a–c display the corresponding top-view and tilt-view SEM images of one metalens with a designed NA of 0.155. It is easy to see that both the solid and inverse meta-units are well produced. Their locations, shapes and feature sizes are strictly in accordance with the numerical design (Fig. 3b). Meanwhile, the Si_3N_4 nanopillars have nearly vertical sidewalls (Fig. 3c), with the measured tilt angle of sidewalls approximately 89–90°. All these results indicates that the designed phase, group delay, and efficiency for an achromatic metalens can be satisfied and realized in real samples.

The optical properties of Si_3N_4 achromatic metalens are optically characterized using a home-made optical system (see Supplementary Fig. S12). The unpolarized supercontinuum laser is collimated and passed through a bandpass filter. The incident beam reaches the metalens from the substrate and is focused. To determine the focal length, the cross-sectional intensity profiles along the propagation direction has been recorded at different wavelengths and shown in Fig. 3d. With the increase of central wavelength from 460 nm to 650 nm, the brightest spots remain at a constant position, which is 97.33 μm away from the Si_3N_4 metalens with a variation of 5%. This focal length matches the numerical designed value (F = 93.5 μm, marked by white dashed line). Figure 3e shows the normalized intensity profiles of the focal spot in x-y plane at different wavelength. The full-widths at half-maximum (FWHMs) of intensity along the diameter of focal spot are very close to the diffraction limit ($\lambda/2NA$, see Supplementary Fig. S16). Meanwhile, the corresponding Strehl ratios remains at a high value of 0.88 across the entire visible spectrum. By measuring the transmitted power at the focal spot and the incident power, the focusing efficiency of metalens has also been measured and plotted in Fig. 1e. An average efficiency of 80.39% has been experimentally obtained across the entire spectral range. This value is a record for visible-light achromatic metalens, but is still slightly lower than the numerically design. Considering the largest reduction occurs at shorter wavelength, this degradation might be caused by three factors, i.e., size variation, imperfect sidewall, and surface roughness and can be potentially improved (details in Supplementary Note 5).

The capability of full-color imaging of achromatic metalens has been experimentally characterized as well. Figure 4a–f shows achromatic imaging of a 1951 United States Air Force (USAF) resolution test chart, highlighting a typical resolvable structure illuminated by lights

https://doi.org/10.1038/s41467-025-62539-7

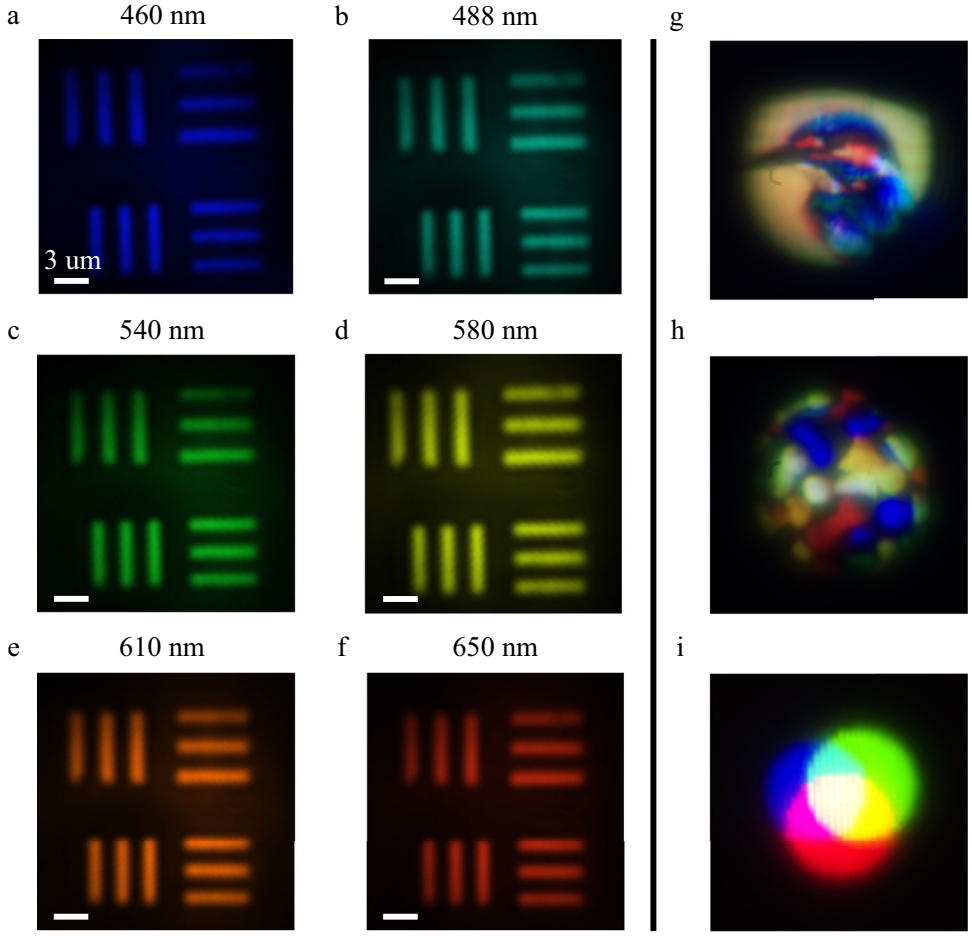

Fig. 4 | Imaging using the achromatic metalens with NA = 0.155. a–f The images of element 5 and 6, group 7 of the 1951 Unites States Air Force resolution target recorded by the achromatic metalens at different wavelengths. The images have the same scale bar. **g–i** The full-color images formed by the achromatic metalens without color correction.

with wavelengths ranging from 460 nm to 650 nm. The smallest resolved feature had a linewidth of 2.19 μm (group 7, element 5 and element 6), determined by the Rayleigh criterion and the measured FWHM shown in Fig. 3e, indicating the precise fabrication of the achromatic metalens. Moreover, the small efficiency variation though the viable wavelength will reduce color differences, enabling the creation of realistic full-color images through our achromatic metalens without compensating the intensity at three preliminary colors. Figure 4g–i present the full-color images formed through our achromatic metalens, captured by a CCD without any additional intensity compensation for three preliminary colors. Compared to the original pictures (available in Supplementary Fig. S17), the color images appeal reliable and closely match originals. The images in Fig. 4 demonstrate the effectiveness of eliminating the chromatic effect across the entire visible spectrum and enable rapid recording of true-color images.

Integration of Si_3N_4 achromatic metalens array on a CMOS chip

Based on the above demonstrations, we further integrate the Si_3N_4 achromatic metalens onto a CMOS image sensor. For a fixed pillar height of 1300 nm, the working principle of achromatic metalens restricts its size and NA to small values. To improve the image quality and fit the commercial device, a 5×5 metalens array have been fabricated and mounted on the chip (Fig. 5a). Figure 5b shows a microscope image of the metalens array at 10× magnification. Each metalens has a diameter of 90 μm. The designed focal length and NA are 980 μm and 0.046, respectively. Then the optical properties of all metalenses have been measured. The average focusing efficiencies, focal lengths and NA values in the visible spectrum are summarized in Fig. 5c–e. The detailed information can be seen in Supplementary Note 9. We can see that all the metalenses have almost identical focal length and NA at the designed values. The average focusing efficiency also remains as a constant around 67% ± 2%.

The high uniformity of the integrated metalens array allows for imaging without color cast. The colorful image can be directly obtained on the imaging plan, located precisely on the CMOS sensor surface. The achromatic metalens array forms 25 sub-images with ~90 μm in size, offering different perspectives of the projected object as shown in Fig. 5f. Each sub-image is clear and easy to distinguish without overlay with each other. A commercial panoramic image stitching software, PTGui, is used to create a high-quality composite image from these sub-images (details in Supplementary Note 10). Figure 5g presents the reconstructed images after correcting color distortion and background subtraction without losing the resolution (5 μm in linewidth of group 6, element 5, as shown in Supplementary Fig. S22). As the object magnification increases, the sensor image can still be directly recorded, producing clear, colorful light-field image that conform our integrated achromatic metalens array can effectively break the restriction between achromatic bandwidth and wide FOV. Since this stitched image covers an area 1.8 times larger than that of a single metalens without decreasing the resolution, efficiency and achromatic performance, the array can be easily expanded to cover much larger areas, potentially encompassing the entire CMOS sensor. The metalens array is further fabricated directly on top of the sensor using Direct Laser Writing to in-situ polymerize a polymer film (details

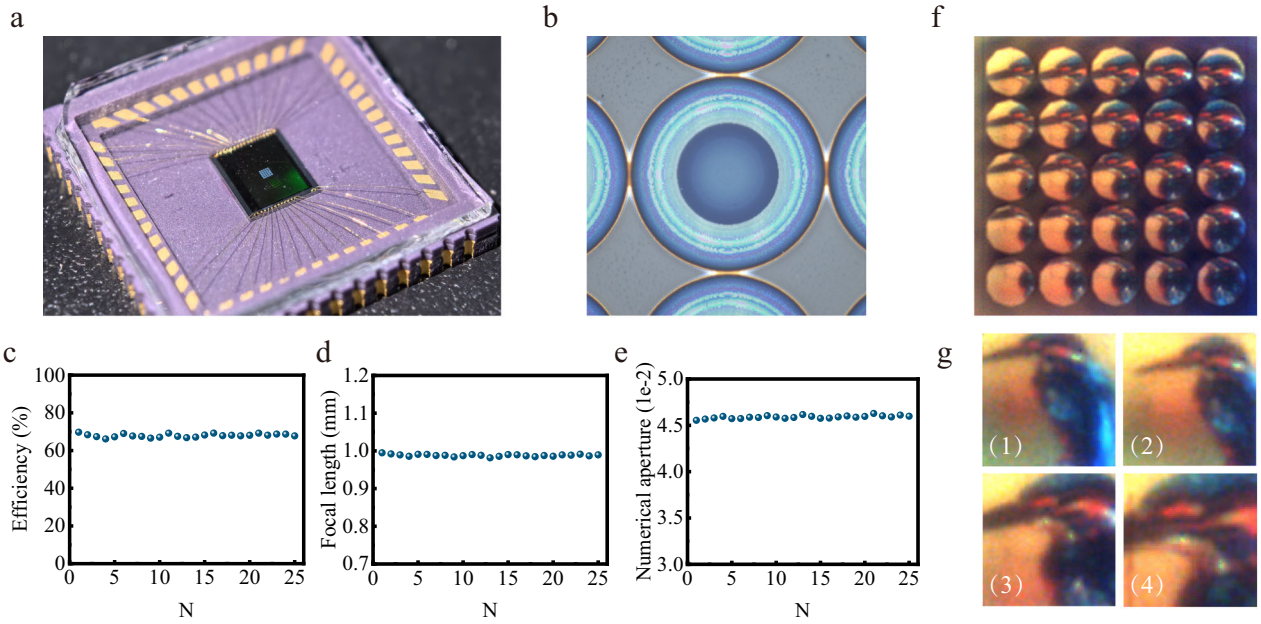

Fig. 5 | Light-field imaging with a metalens array. a The top-view optical microscope images of the metalens array. **b** The high-resolution top-view optical microscope images of single metalens. **c**–**e** are the measured averaged focusing efficiencies, focal lengths and numerical aperture for 25 separated single metalenses. **f** The raw light-field image with the achromatic metalens array. **g** The rendered images with color distortion and background subtraction. (1–4) represent different positions with different magnification rates of the original image respectively.

in Supplementary Note 12), confirming that the deposition of the Si_3N_4 and the etching process have no adverse effect on the performance of the image sensors and the Si_3N_4 meta-units can be well fabricated as designed. This approach can enable wide FOV integral and achromatic imaging through the entire visible wavelength range.

Discussion

In summary, we have developed an approach to fabricate high quality Si_3N_4 achromatic metalens in the visible spectrum. The improved nanofabrication process can produce Si_3N_4 nanostructures with a record-breaking aspect ratio. As a consequence, the group delay range of Si_3N_4 nanopillars are increased and the key performances of metalens in focusing efficiency and NA have been significantly improved too. The nanofabrication techniques are stable and reproducible. Achromatic metalens array with nearly identical performances has been experimentally demonstrated and combined to a commercial CMOS imaging sensor. As a consequence, high performance full color image has been achieved with a single metalens or an integrated metalens array. Since all processes are conducted at low temperature with low electron beam energy, sensor integrity is maintained, ensuring that imaging performance is fully protected. The direct integration of Si_3N_4 meta-units on top of CMOS chip has also been carried out. The integrated achromatic Si_3N_4 metalens array holds promise for the mass manufacture of high-performance, next-generation optical devices based on metasurfaces.

Methods

Numerical simulations

To fulfill the phase compensation requirements for different positions of the metalens, a comprehensive meta-units library with various structural parameters is established. The transmission and phase spectra result for all meta-units are simulated using Reticolo, a rigorous coupled-wave analysis (RCWA) solver. The Si_3N_4 meta-unit has a height of 1300 nm and the meta-unit periodicity is set as 350 nm. For each simulation, a sweep parameter is utilized to obtain the phase spectrum, with the wavelength varying from 460 nm to 650 nm. A linear fit is utilized to analyze the phase spectrum in order to calculate the group delay and the spectral reference phase at the zero frequency. To demonstrate the focusing performance of the achromatic metalens, finite-domain time-difference simulations (Lumerical FDTD Solutions) are utilized to model the metalens. Perfectly matched layer (PML) boundary conditions are applied along both transverse and longitudinal directions under plane wave illumination.

Film deposition

The 1300-nm-thick high-quality Si_3N_4 film is deposited onto the K9 optical glass substrate with plasma enhanced chemical vapor deposition (PECVD) in a mixture of SiH_4, NH_3 and N_2 gas. The deposition rate is 6.5 nm/min and the deposition temperature is 200 °C. The optical parameters are measured using spectroscopic ellipsometer and shown in Supplementary Fig. S5. By adjusting the silicon-nitrogen ratio during deposition, the refractive index of the film can be obtained to be approximately 2.02 through the whole visible wavelength, while the loss can be ignored.

Device fabrication

After the deposition of Si_3N_4 film, 50-nm-thick Cr layer is deposited on the film used the E-beam evaporator. Subsequently, the PMMA A2 e-beam resist is spin-coated onto the Cr layer and baked at 180 °C for 15 min. The sample is then exposed through the electron-beam lithography system (Raith E-line Plus) and the patterns are revealed after the development process in MIBK/IPA. Following this, 20-nm-thick SiO_2 layer is deposited as hard mask to etch the Cr layer on the sample using the E-beam evaporator. The pattern is transferred to SiO_2 through a lift-off process using PG Remover. Next, the patterns are transferred to the Cr layer by inductively coupled plasma etching (Oxford PlasmalabSystem100, ICP180) in a mixture of Cl_2 and O_2 gas. The patterns are then transferred to Si_3N_4 film using Cr as the hard mask by ICP in a mixture of CHF_3 and O_2 gas. As the etching depth increases, adjustments are made to the ratio of CHF_3/O_2 from 12.5 to 7.2, effectively improving anisotropic etching and achieving high

aspect ratio silicon nitride meta-units etching. The final metalens can be obtained after removal of the Cr hard etching mask.

Optical characterization

In order to verify the performance of the broadband achromatic metalens, we built a home-made optical system. Details of the optical experimental setup for characterizing the broadband achromatic metalens are shown in Supplementary Note 6. The sample is moved 0.1 μm per step by a motion control module (Kinesis® K-Cube) controlled by Labview to record the intensity distributions along z-axis.

For the purpose of accurately evaluating the focusing efficiency of the metalens, we measured the power concentrated in the focal spot. This is determined by measuring the power of the transmitted light that passed through a circular area with a radius of 3×FWHM of the focal spot. We then divide this by the power of the incident light, which is measured as the power of the incident light passing through a circular area with the same radius as the metalens.

Data availability

The data that support the plots within this paper and other findings of this study are available from the corresponding author on request.

Code availability

The code that supports the plots within this paper and other findings of this study are available from the corresponding author on request.

References

1. Lee, G.-Y. et al. Metasurface eyepiece for augmented reality. *Nat. Commun.* **9**, 4562 (2018).
2. Pahlevaninezhad, H. et al. Nano-optic endoscope for high-resolution optical coherence tomography in vivo. *Nat. Photonics* **12**, 540–547 (2018).
3. Chen, C. et al. Spectral tomographic imaging with aplanatic metalens. *Light Sci. Appl.* **8**, 99 (2019).
4. Li, Z. et al. Meta-optics achieves RGB-achromatic focusing for virtual reality. *Sci. Adv.* **7**, eabe4458 (2021).
5. Malek, S. C., Overvig, A. C., Alù, A. & Yu, N. Multifunctional resonant wavefront-shaping meta-optics based on multilayer and multi-perturbation nonlocal metasurfaces. *Light Sci. Appl.* **11**, 246 (2022).
6. Wang, C. et al. Miniature two-photon microscopic imaging using dielectric metalens. *Nano Lett.* **23**, 8256–8263 (2023).
7. Choi, M. et al. Roll-to-plate printable RGB achromatic metalens for wide-field-of-view holographic near-eye displays. *Nat. Mater.* **24**, 535–543 (2025).
8. Fröch, J. E. et al. Beating spectral bandwidth limits for large aperture broadband nano-optics. *Nat. Commun.* **16**, 3025 (2025).
9. Barulin, A. et al. Axially multifocal metalens for 3D volumetric photoacoustic imaging of neuromelanin in live brain organoid. *Sci. Adv.* **11**, eadr0654 (2025).
10. Pendry, J. B. Negative refraction makes a perfect lens. *Phys. Rev. Lett.* **85**, 3966–3969 (2000).
11. Yu, N. et al. Light propagation with phase discontinuities: generalized laws of reflection and refraction. *Science* **334**, 333–337 (2011).
12. Kamali, S. M., Arbabi, E., Arbabi, A. & Faraon, A. A review of dielectric optical metasurfaces for wavefront control. *Nanophotonics* **7**, 1041–1068 (2018).
13. Fan, Z.-B. et al. A broadband achromatic metalens array for integral imaging in the visible. *Light Sci. Appl.* **8**, 67 (2019).
14. Chen, W. T., Zhu, A. Y., Sisler, J., Bharwani, Z. & Capasso, F. A broadband achromatic polarization-insensitive metalens consisting of anisotropic nanostructures. *Nat. Commun.* **10**, 355 (2019).
15. Xu, B. et al. Metalens-integrated compact imaging devices for wide-field microscopy. *Adv. Photonics* **2**, (2020).
16. Wang, Y. et al. High-efficiency broadband achromatic metalens for near-IR biological imaging window. *Nat. Commun.* **12**, 5560 (2021).
17. Shastri, K. & Monticone, F. Bandwidth bounds for wide-field-of-view dispersion-engineered achromatic metalenses. *EPJ Appl. Meta.* **9**, 16 (2022).
18. Zhang, L. et al. High-efficiency, 80 mm aperture metalens telescope. *Nano Lett.* **23**, 51–57 (2023).
19. Peng, Y. et al. Metalens in improving imaging quality: advancements, challenges, and prospects for future display. *Laser Photonics Rev.* **18**, 2300731 (2024).
20. Arbabi, E., Arbabi, A., Kamali, S. M., Horie, Y. & Faraon, A. Multiwavelength polarization-insensitive lenses based on dielectric metasurfaces with meta-molecules. *Optica* **3**, 628–633 (2016).
21. Khorasaninejad, M. & Capasso, F. Metalenses: versatile multifunctional photonic components. *Science* **358**, eaam8100 (2017).
22. Hu, Y. et al. Asymptotic dispersion engineering for ultra-broadband meta-optics. *Nat. Commun.* **14**, 6649 (2023).
23. Lin, R. J. et al. Achromatic metalens array for full-colour light-field imaging. *Nat. Nanotechnol.* **14**, 227–231 (2019).
24. Chen, W. T. et al. A broadband achromatic metalens for focusing and imaging in the visible. *Nat. Nanotechnol.* **13**, 220–226 (2018).
25. Wang, S. et al. A broadband achromatic metalens in the visible. *Nat. Nanotechnol.* **13**, 227–232 (2018).
26. Hua, X. et al. Ultra-compact snapshot spectral light-field imaging. *Nat. Commun.* **13**, 2732 (2022).
27. Li, Z. et al. Inverse design enables large-scale high-performance meta-optics reshaping virtual reality. *Nat. Commun.* **13**, 2409 (2022).
28. Ye, X. et al. Chip-scale metalens microscope for wide-field and depth-of-field imaging. *Adv. Photonics* **4**, (2022).
29. Mathews, N. R., Morales, E. R., Cortés-Jacome, M. A. & Toledo Antonio, J. A. TiO2 thin films – Influence of annealing temperature on structural, optical and photocatalytic properties. *Sol. Energy* **83**, 1499–1508 (2009).
30. Abdullaev, O. et al. MOCVD growth GaN on sapphire. *IOP Conf. Ser. Mater. Sci. Eng.* **617**, 012015 (2019).
31. Karouta, F., Vora, K., Tian, J. & Jagadish, C. Structural, compositional and optical properties of PECVD silicon nitride layers. *J. Phys. Appl. Phys.* **45**, 445301 (2012).
32. Yang, C. & Pham, J. Characteristic study of silicon nitride films deposited by LPCVD and PECVD. *Silicon* **10**, 2561–2567 (2018).
33. Gardes, F. et al. A review of capabilities and scope for hybrid integration offered by silicon-nitride-based photonic integrated circuits. *Sensors* **22**, 4227 (2022).
34. Xiang, C., Jin, W. & Bowers, J. E. Silicon nitride passive and active photonic integrated circuits: trends and prospects. *Photonics Res.* **10**, A82–A96 (2022).
35. Buzaverov, K. A. et al. Silicon nitride integrated photonics from visible to mid-infrared spectra. *Laser Photonics Rev.* **18**, 2400508 (2024).
36. Colburn, S., Zhan, A. & Majumdar, A. Metasurface optics for full-color computational imaging. *Sci. Adv.* **4**, eaar2114 (2018).
37. Tseng, E. et al. Neural nano-optics for high-quality thin lens imaging. *Nat. Commun.* **12**, 6493 (2021).
38. Miyata, M., Nemoto, N., Shikama, K., Kobayashi, F. & Hashimoto, T. Full-color-sorting metalenses for high-sensitivity image sensors. *Optica* **8**, 1596 (2021).
39. Li, H. et al. Bandpass-filter-integrated multiwavelength achromatic metalens. *Photonics Res.* **9**, 1384 (2021).
40. Gao, H. et al. Dynamic 3D meta-holography in visible range with large frame number and high frame rate. *Sci. Adv.* **6**, eaba8595 (2020).
41. Ren, H. et al. Metasurface orbital angular momentum holography. *Nat. Commun.* **10**, 2986 (2019).

42. Presutti, F. & Monticone, F. Focusing on bandwidth: achromatic metalens limits. *Optica* **7**, 624 (2020).
43. Chen, Q., Gao, Y., Pian, S. & Ma, Y. Theory and fundamental limit of quasiachromatic metalens by phase delay extension. *Phys. Rev. Lett.* **131**, 193801 (2023).

Acknowledgements

This research was supported by National Key Research and Development Program of China: (Grant Nos. 2023YFB2806704, 2022YFA1404700, and 2021YFA1400802), National Natural Science Foundation of China (Grant Nos. 62125501, 12025402, 11974092, 61975041, and 12261131500), Shenzhen Fundamental Research Project (Grant Nos. JCYJ20220818102218040 and JCYJ20241202123729038, JCYJ20241202123719025), Fundamental Research Funds for Central Universities (Grant Nos. 2022FRRK030004).

Author contributions

Q.S. and S.X. conceived the idea and supervised the research. Y.Z. and G.Q. did the design. Y.Z., X.J., C.L. and Q.R. fabricated the samples. Y.Z. performed the experimental measurements. J.H., B.B. and Z.L. revised the manuscript and figures. S.X. and Q.S. analyzed the results. All the authors discussed the contents and prepared the manuscript.

Competing interests

The authors declare no competing interests.

Additional information

Supplementary information The online version contains supplementary material available at https://doi.org/10.1038/s41467-025-62539-7.

Correspondence and requests for materials should be addressed to Qinghai Song or Shumin Xiao.

Peer review information *Nature Communications* thanks Masashi Miyata, Junsuk Rho and the other anonymous reviewer(s) for their contribution to the peer review of this work. A peer review file is available.